Copyright © 2011 Tech Science Press CMC, vol.22, no.1, pp.73-95, 2011

Numerical Simulation of Detonation and Multi-Material Interface Tracking

Cheng Wang[1], Jianguo Ning[1] and Tianbao Ma[1]

Abstract: In this paper, we report high resolution simulations using a fifth-order weighted essentially non-oscillatory (WENO) scheme with a third-order TVD Runge–Kutta time stepping method to examine the features of the detonation for gas and condensed explosives. A two-stage chemical reaction model and an ignition and growth model are employed to describe the chemical reaction process for gas and condensed explosives. Based on the Steger-Warming vector flux splitting method, a splitting method is employed when the vector flux does not satisfy the homogeneity property for simulating detonation wave propagation for condensed explosives. The sensibility of flame propagation process and explosion overpressure on obstacles is also numerically performed. Meanwhile, an interface tracking algorithm is developed and coupled with a two-dimensional multi-material code indigenously for simulating the response of materials to impact, shocks and detonations. Numerical experiments are performed to investigate the influences of liner cone angle, wall thickness and initiation mode on shaped charge jet formation process. The results of calculations show good agreement with experimental results, and indicate that the interface treatment algorithm is especially suitable for simulating explosive loading on thin-wall structure such as shape charges.

Keywords: Detonation; Interface tracking, WENO, Condensed explosive; Obstacles

1 Introduction

Detonation and the material dynamic response under detonation load are highly nonlinear phenomena. It is hard to describe these problems by analytical solutions. Hence we have to seek numerical methods. However, two main challenges are still confronted in the numerical methods: the numerical scheme of the governing equations for detonation and the special treatments for the material interfaces.

[1] State Key Laboratory of Explosion Science and Technology, Beijing Institute of Technology, Beijing 100081, P.R.China

The numerical simulation for Deflagration-to-detonation transition(DDT) in channels with obstacles is still an active research area due to its practical importance. Vaagsaether et al. explored the effect of obstacles on flame propagation and DDT by a numerical code based on a 2nd order accurate total variation diminishing (TVD), flux limiter centered scheme [Vaagsaether, Knudsen and Bjerketvedt (2007)]. Gamezo et al. studied flame acceleration and DDT in channels with obstacles using an explicit, second-order, Godunov-type numerical scheme. The energy release rate for the stoichiometric H_2-air mixture is modeled by a one-step Arrhenius kinetics [Gamezo, Ogawa and Elaine (2007)]. Furthermore, they investigated the influences of obstacle spacings and configurations on flame acceleration and DDT phenomena [Gamezo, Ogawa and Elaine (2008)].

For condensed explosives simulation, Stewart et al. presented an integrated algorithm on a Eulerian grid for simulating the interaction of energetic and inert materials [Stewart, Yoo and Wescott (2007)]. Xu et al. developed a high-resolution, multidimensional Euler solver which is capable of handling non-ideal equation of state and stiff chemical source terms for simulating DDT in porous energetic materials [Xu, Aslam and Stewart (1997)]. Kapilia et al. adopted a second-order, Godonov-type, shock-capturing scheme which has been extended to handle the mixture Jones-Wilkins-Lee(JWL) equation of state and the multi-stage reaction rate for the ignition-and-growth model to simulate detonation diffraction [Kapila, Schwendeman, Bdzil and Henshaw (2007)].

The efficient approaches for the simulation of high-strain rate, large deformation problems resulting from detonation load are Eulerian method [Benson (1995); Tran and Udaykumar(2004) ; Ma, Wang and Ning (2008); Wang, Liu and Zhang (2009)] and meshless method. Recently developed meshless methods show much advantage for problems with very large deformation, such as condensed explosives detonation and consequent demolishment to the structures. Atluri et al (2002) proposed a general framework for developing the Meshless Local Petrov-Galerkin (MLPG) approach. As an extension, a meshless mixed finite volume method is proposed [Atluri, Han and Rajendran (2004), Han, Rajendran and Atluri (2005)] to further simplify the meshless formulations. Han et al (2006) developed a three-dimensional dynamic code based on MLPG approach. The ability of the MLPG code for solving high-speed contact, impact and penetration problems with large deformations and rotations is demonstrated through the Taylor impact problem and perforation problems. The computational times are recorded and compared with those of the popular finite element code (Dyna3D) to demonstrate the efficiency of the present MLPG approach. Campbell et al (2009) investigated the interaction of large ocean waves with ships and offshore structures specifically with respect to the extent of deck submersion, impact loads and the level of structural dam-

age by using an explicit coupled Smooth Particle Hydrodynamics (SPH) and finite element approach. Material point method (MPM), which is a special case of MLPG, is an efficient meshfree particle method for solving continuum problem. Huang et al (2008) employed MPM to investigate hypervelocity impact for obtaining the high-resolution results of debris cloud. Ma et al(2009) developed a three dimensional MPM3DPP code using adaptive MPM to simulate different explosion problems including explosively driven flyer and shaped charge problems. Shen (2009) investigated glass fragmentation under impact loading by means of MPM. Recently, Bardenhagen et al (2004) developed a generalized Interpolation Material Point (GIMP) method based on Petrov-Galerkin discretization scheme. Ma et al (2005) performed multiscale simulations on a 2D nanoindentation problem by GIMP.

On the other hand, it is difficult to identify the material interfaces accurately at each time step. Therefore, the interface tracing algorithm must be adopted for the Eulerian approach. At present, there are a lot of interface treatment methods by adopting techniques in the arsenal of computational fluid dynamics [Hirt and Nichols (1981);Benson (1995); Osher and Sethian (1998); Rider and Kothe (1998); Fedkiw, Aslam, Merriman and Osher (1999); Liu, Khoo and Yeo (2003); Wen (1998); Tran and Udaykumar(2004); Ma, Wang and Ning (2008); Wang, Liu and Zhang (2009);. Wang, Huang and Ning (2009)].

In the present work, high resolution fifth-order WENO scheme with a third-order TVD Runge–Kutta method is employed to investigate the influences of spacing and blockage ratio on flame propagation and explosion overpressure. A splitting method is employed when the vector flux does not satisfy the homogeneity property for simulating detonation wave propagation for condensed explosives. An interface tracking algorithm is proposed and coupled with a two-dimensional Hydro-Elastoplastic code indigenously to simulate shaped charge jet formation process. The numerical results for detonation and shaped charge jet show good agreement with the experimental results.

2 Numerical Simulations of detonation

2.1 Governing equations

Numerical experiments have been performed by two-dimensional Euler equations with chemical reaction model. A two-stage chemical reaction model [Fujiwara and Taki (1978)] for gas detonation and an ignition and growth model [Lee and Tarver (1980)] for condensed explosives are employed. Without considering viscosity, heat conductance and dissipation, the governing equations are given as follows:

$$U_t + F(U)_x + G(U)_y = S(U)$$

For gas detonation:

$$U = (\rho, \rho u, \rho v, \rho E, \rho \alpha, \rho \beta)^T$$

$$F(U) = \left(\rho u, \rho u^2 + p, \rho uv, \rho u(E + p/\rho), \rho u\alpha, \rho u\beta\right)^T$$

$$G(U) = \left(\rho v, \rho vu, \rho v^2 + p, \rho v(E + p/\rho), \rho v\alpha, \rho v\beta\right)^T$$

$$S(U) = \left(0, 0, 0, 0, \rho \omega_\alpha, \rho \omega_\beta\right)^T$$

$$E = e + \beta q + \frac{1}{2}\vec{V}^2$$

$$\omega_\alpha = \frac{d\alpha}{dt} = -k_1 \rho \exp(-E_1/RT)$$

$$\omega_\beta = \frac{d\beta}{dt} = \begin{cases} 0, & (\alpha > 0) \\ -k_2 p^2 [\beta^2 \exp(\frac{-E_2}{RT}) - (1-\beta)^2 \exp(-\frac{E_2+q}{RT})], & (\alpha \le 0) \end{cases}$$

For condensed phase detonation:

$$U = (\rho, \rho u, \rho v, \rho E, \rho \lambda)^T$$

$$F(U) = \left(\rho u, \rho u^2 + p, \rho uv, \rho u(E + p/\rho), \rho u\lambda\right)^T$$

$$G(U) = \left(\rho v, \rho vu, \rho v^2 + p, \rho v(E + p/\rho), \rho v\lambda\right)^T$$

$$S(U) = \left(0, 0, 0, 0, \rho \dot{\lambda}\right)^T$$

$$E = e + (1-\lambda)\,q + \frac{1}{2}\vec{V}^2$$

$$\dot{\lambda} = I(1-\lambda)^{2/9}\eta^4 + G(1-\lambda)^{2/9}\lambda^{2/3}p^Z$$

where $\vec{V}$ is the velocity vector, E is the total energy of unit mass, p is pressure, q is the heat generated by the reaction with unit mass of reactants, α and β are the reaction progress parameters in the induction and exothermic periods, respectively, and E_2 are the activation energy, k_1 and k_2 are the preexponential factors, IGZ are constants, λ is the mass fraction of the reaction product, υ_0 is the specific volume of explosive at initial time, υ_1 is the specific volume of explosive and $\eta = \upsilon_0/\upsilon_1 - 1$. For the detonation of gas, the equation of state for ideal gas is employed. We take JWL equation of state for both explosive and reaction product [Ma, Wang and Ning (2008)].

2.2 Numerical Method

Flux is decomposed by adopting Steger-Warming vector flux splitting method. The above Eulerian equations with the equation of state for ideal gas satisfy the homogeneity property, while with the JWL equation of state, they do not have the same property. Therefore, the Steger-Warming splitting method [Steger and Warming (1981)] cannot be directly used for JWL equation of state. However, we can borrow the concept of the Steger-Warming flux splitting and make minor revisions to achieve the vector flux splitting. Take the vector flux F at x direction as an example.

$$\begin{aligned} F &= F^+ + F^- + \Delta F \\ &= (F_1^+ + F_2^+ + F_3^+) + (F_1^- + F_2^- + F_3^-) + \Delta F \end{aligned}$$

where ΔF is the revision item. For gas detonation:

$$F_1^{\pm} = \frac{\rho\frac{((u-c)\pm\max|u-c|)}{2}}{2\gamma}(1, u-c, v, h-uc, \beta, \alpha)^T$$

$$F_2^{\pm} = \frac{\rho\,(\gamma-1)\,\frac{(u\pm\max|u|)}{2}}{\gamma}(1, u, v, \tfrac{1}{2}\vec{V}^2 + \beta q, \beta, \alpha)^T$$

$$F_3^{\pm} = \frac{\rho\frac{((u+c)\pm\max|u+c|)}{2}}{2\gamma}(1, u+c, v, h+uc, \beta, \alpha)^T$$

$$\Delta F = (0,0,0,0,0,0)^T$$

For condensed explosives detonation:

$$F_1^{\pm} = \frac{\rho \frac{((u-c)\pm\max|u-c|)}{2}}{2\gamma}(1, u-c, v, h-uc, \lambda)^T$$

$$F_2^{\pm} = \frac{\rho(\gamma-1)\frac{(u\pm\max|u|)}{2}}{\gamma}(1, u, v, \tfrac{1}{2}\vec{V}^2+\beta q, \lambda)^T$$

$$F_3^{\pm} = \frac{\rho \frac{((u+c)\pm\max|u+c|)}{2}}{2\gamma}(1, u+c, v, h+uc, \lambda)^T$$

$$\Delta F = \left(0, p-\frac{\rho c^2}{\omega+1}, 0, 0, 0, 0\right)^T$$

Similarly, the splitting results of vector flux G at $y$direction can be obtained.

Thus, the semi-discrete conservation scheme for governing equations is:

$$\left(\frac{\partial U}{\partial t}\right)_{i,j} = -\frac{1}{\Delta x}\left(\hat{F}^+_{i+1/2,j} - \hat{F}^+_{i-1/2,j}\right) - \frac{1}{\Delta x}\left(\hat{F}^-_{i+1/2,j} - \hat{F}^-_{i-1/2,j}\right) - \frac{1}{\Delta y}\left(\hat{G}^+_{i,j+1/2} - \hat{G}^+_{i,j-1/2}\right) - \frac{1}{\Delta y}\left(\hat{G}^-_{i,j+1/2} - \hat{G}^-_{i,j-1/2}\right) - S_{i,j}$$

where, $\hat{F}^{\pm}_{i\pm1/2,j}$ and $\hat{G}^{\pm}_{i,j\pm1/2}$ are the numerical flux at cell boundary and can be evaluated by means of WENO scheme [Jiang and Shu (1996); Shu (2009)]. For temporal discretization, the third order Runger-Kutta method is adopted in this paper.

2.3 Numerical Simulations of Gas detonation

The flame propagation process for hydrogen dominated mixture in a 80mm-diameter and 20m-long duct is simulated. On the left of the duct, a segment of high-temperature gas is initially set for simulating ignition. In all numerical experiments, the flame propagation velocity at different times is denoted by D/D_{CJ}(where D_{CJ} is the velocity for detonation wave). Time is also denoted by T/t^* (t^* is time of induced reaction). Further denote blockage ratio as $B = (L^2 - \pi r^2)/L^2$, in which r is the inner radius of obstacle circle, and L the inner side length of the duct.

1) Influence of spacing of obstacles on detonation

Under the condition of the same blockage ratio and plate number, the influence of plates spacing on detonation wave are investigated. The spacing ranges from

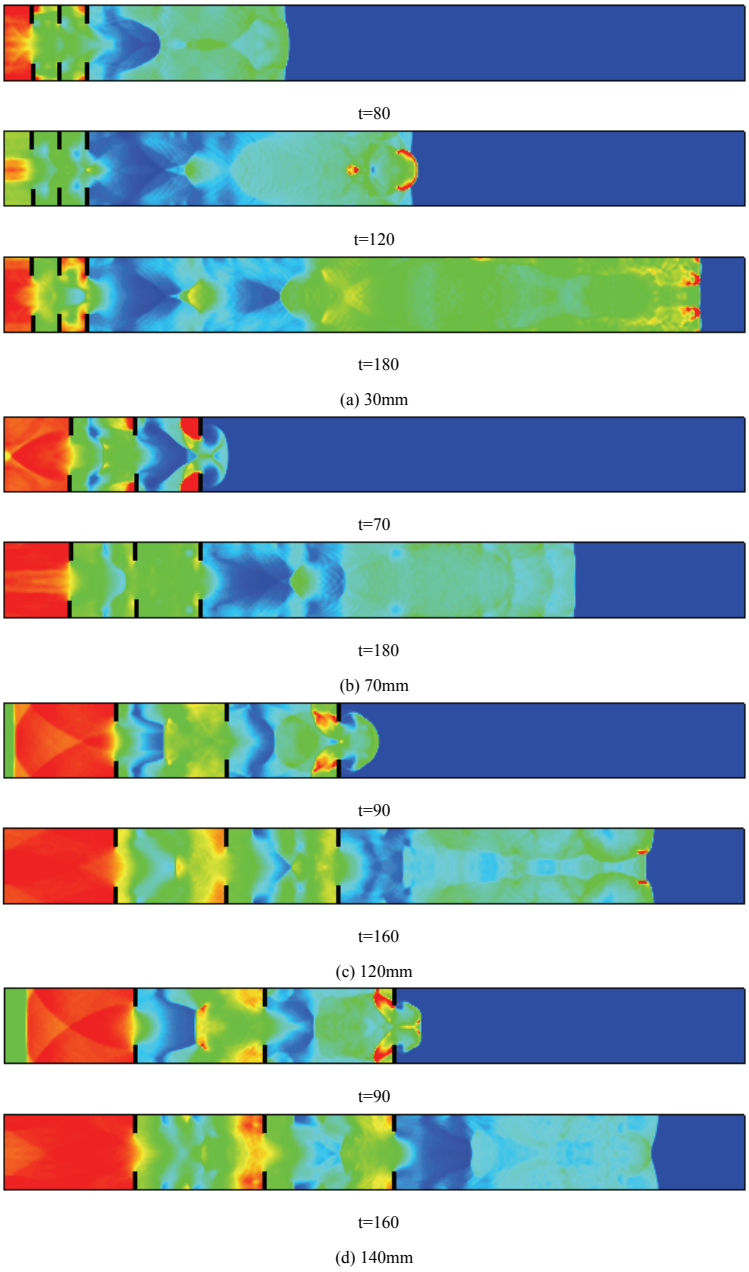

Figure 1: Propagation process of detonation wave for different plates spacing

30mm, 50mm, 70mm, 120mm and 140mm. Fig.1 shows the propagation process of detonation wave at spacing of 30mm, 70mm, 120mm and 140mm, respectively.

It can be observed from Fig.1 that, when the spacing between obstacles is 30mm, secondary blasting phenomenon occurs, which exactly coincides with the retonation phenomenon observed in the experiment [Sun and Zhu (1995)]. This can be explained by the fact that compression waves continuously are produced and track leading shock wave in the process of propagation of wave, and meanwhile reflection takes place on the wall in the process of tracking. Due to such reflection, adequate energy is gathered after the shock wave front, explosion occurs under critical ignition condition, and combines with the reaction zone and self-sustaining supersonic detonation wave is formed.

The propagation velocity of detonation wave variation with time for 30mm, 70mm, 120mm and 140mm are illustrated in Fig.2, respectively. It can be seen from Fig.2a that, due to blocking of the obstacles, the velocity of wave front sharply declines, and the velocity does not recover to nearby 1 until the wave propagates outside the zone of the obstacles. When time ranges between 50 and 120, the value of velocity fluctuates nearby 1 and no triple point is produced. When time comes close to 120, explosion occurs in the center of the duct, pressure suddenly rises, and explosion wave propagates forward and backward, separately. Moreover, when combining with precursor shock wave, detonation wave is formed and propagates in a self-sustained way. Detonation is of the typical triple point structure that contains Mach stem, transverse wave and leading shock wave,

When plane detonation wave passes through the obstacles, energy converges on the central location, equivalent to the start portion of the cellular structure. Shock wave will develop toward both sides and is reflected on the wall surface. Reflection is also one of the key factors that contribute to ignite and sustain development of detonation wave. When the spacing between the obstacles is about 110mm, which is near the cellular size, there is space enough for detonation wave to grow. When the shock wave travels transversely to the next obstacle, it exactly converges on the center of the duct, so the wave can smoothly get past the obstacles when the spacing of the obstacles is 100mm and 120mm. Nevertheless, when the spacing of the obstacles is 50mm, this shock wave traveling transversely is just blocked at the corner between the obstacles and wall surface. The high temperature and pressure energy produced from reflection can in no way transmit to the unburned gas, but most of it can only dissipate in the explosive product zone. Thus, energy loss is significant, which makes detonation wave extinguish. When the spacing of the obstacles are 70mm and 140mm, respectively, the movement of transverse shock wave is also blocked by the obstacles to some extent. Though the velocity of wave front is higher, detonation wave can not come into existence. Therefore, the

relationship between the spacing of the obstacles $d$and cellular length λ meets the following condition, detonation wave can propagate in a self-sustained way.

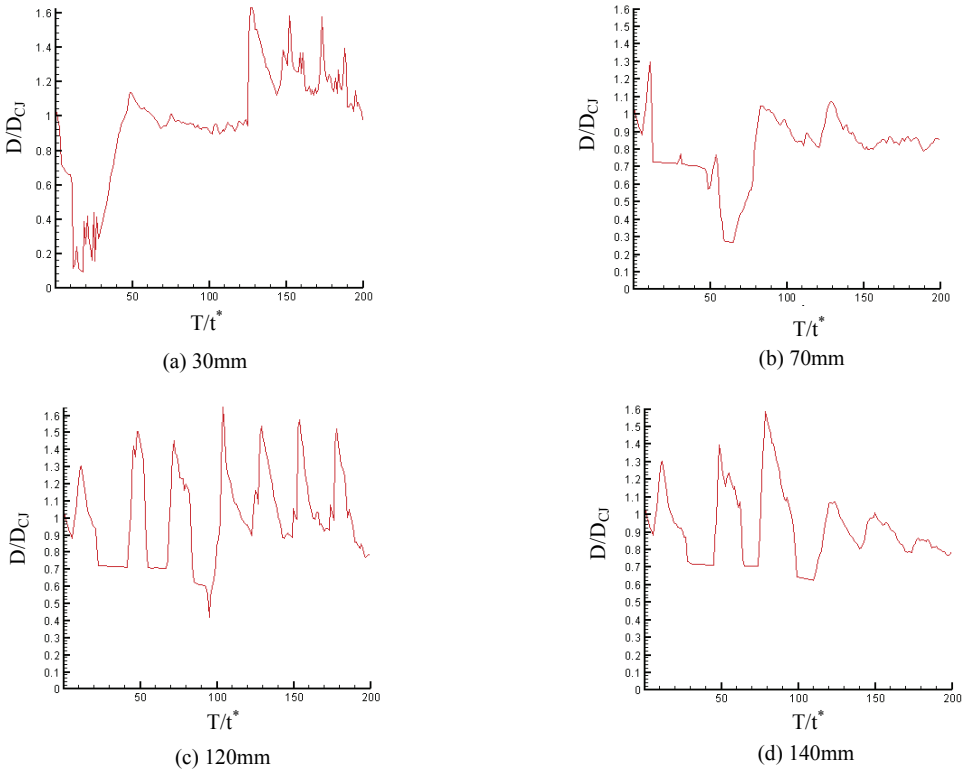

Figure 2: Propagation velocity of detonation wave for different plates spacing

2) Effect of blockage ratio of obstacles on detonation

To investigate the influence of the blockage ratio on flame acceleration, numerical simulations for blockage ratios of 0.83, 0.77, 0.68, 0.57, 0.44, 0.28 are performed under the condition of the same obstacles number and spacing. Fig.3 illustrates the propagation process of detonation wave for 0.77 and 0.57, respectively. Transverse wave variation process is shown in Fig.4. Fig.5 and Fig.6 respectively demonstrate the numerical simulation and experimental results for the propagation speed of the flame and explosion overpressure in the duct. It can be known from the figures that, the numerical simulation results are fairly in good agreement with the experimental ones.

The regression analysis of the data reveals the relationships of the propagation

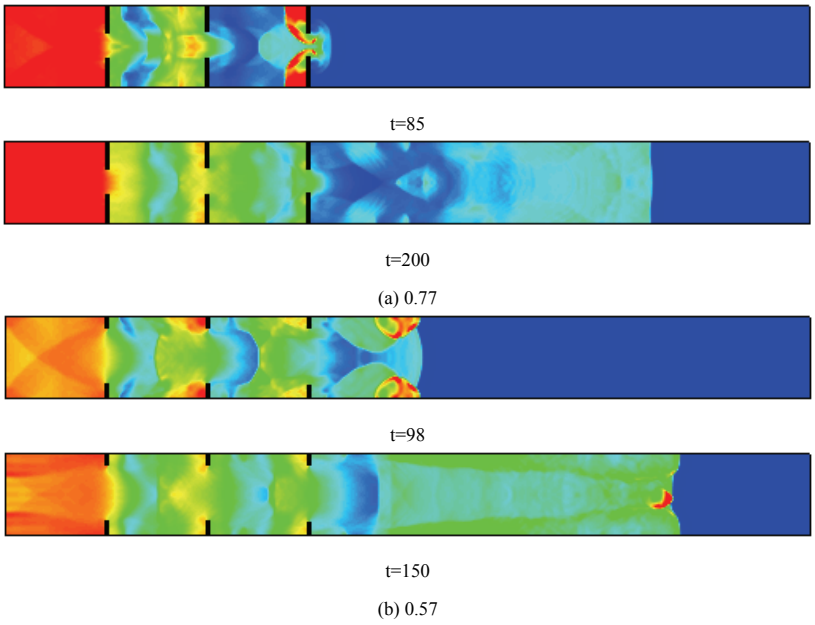

Figure 3: Propagation process of detonation wave for different blockage ratio

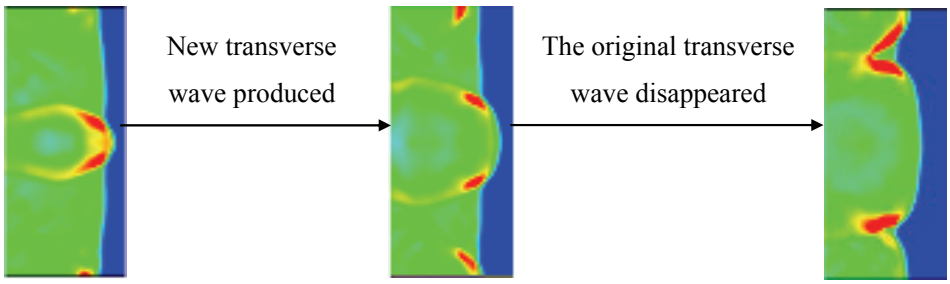

Figure 4: Variation process of transverse wave

speed of the flame and explosion overpressure with blockage ratio in the way as

$$D = -5124.9 + 33097.6B - 54707.7B^2 + 27181B^3$$

$$P = 4.19 + 5.12B - 5.83B^2 + 5.75B^3$$

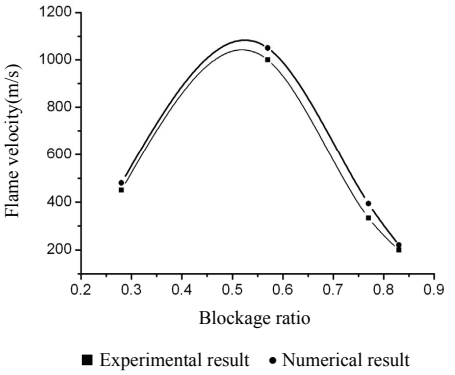

Figure 5: Variation of flame velocity with blockage ratio

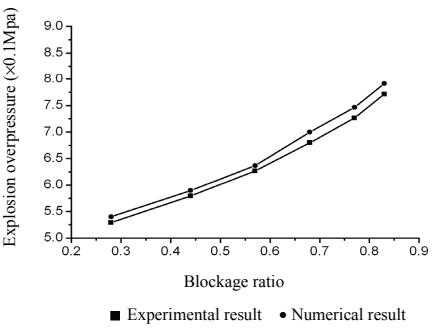

Figure 6: Variation of explosion overpressure with blockage ratio

where D is the propagation velocity of the flame, P is explosion overpressure, and B is blockage ratio.

As shown in Fig.3 and Fig.4, when the blockage ratio is 0.77, detonation wave extinguishes after it passes through the obstacles. When the blockage ratio is 0.57, it can be seen from Fig.3b that transverse wave and cellular structure become unstable, part of the original transverse wave disappears after it collides with the wall surface or another transverse wave, whilst new transverse wave will continuously be produced at the intersection of reflected shock wave, as shown in Fig.4. Instability of transverse wave leads to unevenness and irregularity of cellular structure. It is found in the experiment that such phenomenon is temporary, and both transverse wave and cellular structure will ultimately arrive to stable state, and hence self-sustained detonation wave can emerge.

It can be noted from Fig.5 and Fig.6 that, as the blockage ratio increases, flame velocity increases. Explosion overpressure tends to rise in general. This is due to the increase of blockage ratio, the effect generated by obstacles intensifies, flame velocity increases, and the resulting explosion overpressure on the downstream of the obstacles increases, too. However, when blockage ratio is increased to a certain value, flame velocity begins to drop, and even flame extinguishes. This can be explained by the fact that flow velocity of the mixture before obstacles decreases when blockage ratio increase, which decreases flame velocity, too. Although the flame velocity still increases as blockage ratio increases as a result of combustion velocity increase, the increment of the mixture flow velocity is lower than the decrement, hence flame velocity ultimately decreases. As a result, cold unburned

mixture after obstacles may not be ignited after hot combustion products passing through obstacles, which leads to flame extinguishment.

2.4 Numerical Simulation of condensed phase detonation

Assume the computation domain is 4cm×1cm. The explosive PBX9404 is initiated with CJ state quantity in the area of 0.5cm×1cm, and the remaining part is non-reacting explosive. The grid is divided into 30cells/mm. For the upper and lower boundary condition, continuous boundary conditions are used. Fig.7 demonstrates the distributions of density and pressure at different times when the detonation waves propagate, respectively. The times corresponding to each curve from the left to the right are t=0.596μs, t=1.192μs, t=1.788μs, t=2.384μs, t=2.98μs and t=3.576μs, respectively.

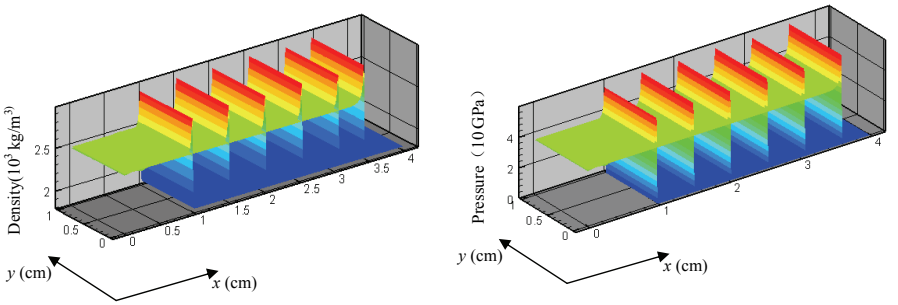

Figure 7: Density and pressure distributions for detonation wave at different times

It can be found from the numerical results that, at first, leading shock wave impacts and condenses un-reacted explosive, density and pressure rapidly rise, reaching Von Neumann peak value. When the temperature and pressure arrive to a certain degree, high-speed chemical reaction is induced. Along with the chemical reactions, large quantities of energy are released. Following that, detonation wave tends towards a stable state, and all physical quantities maintain CJ state. The numerical results accord with actual physical process very well, which indicates a splitting method presented in the paper when the vector flux does not satisfy the homogeneity property is feasible.

3 Multi-material interface tracking algorithm and its application

3.1 Interface tracking algorithm

The basic idea of algorithm is that the interface curve of each material is traced by a series of straight-line segments which connects heads and tails. These segments are called marker lines. The end points of each straight-line segment are located on the grid lines[Wen (1998); Wang, Huang and Ning (2009)]. Thus each material mass, momentum and internal energy between neighboring grids can be advected according to the location of the marker lines in the grid.

1) Markers definition

For a given initial geometric configuration, the intersection points between the boundaries of materials and grid lines serve as a set of massless markers. These markers are numbered in the sequence and the corresponding coordinates for each marker can be calculated. As shown in Fig.8, the interface of a given material is defined by connecting the corresponding markers in turn.

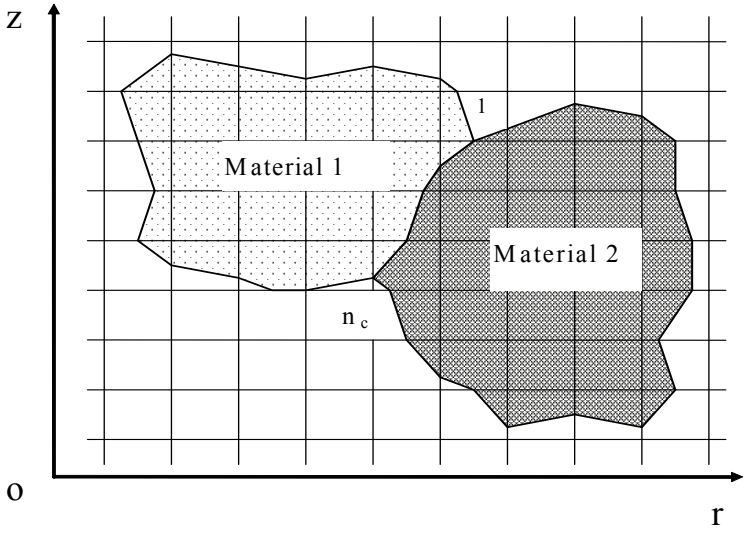

Figure 8: Material packages in computational domain

2) Calculation procedures of markers

To define the position of the markers at time t_{n+1}, First, centering around a given marker, a virtual grid, that is the same as the grid which the marker locates at, is made to cover all Eulerian grids. Velocity components $u$and$v$ at time t_n can be

obtained by interpolation using a weighted average of the velocities and areas for each Eulerian grid:

$$u = \frac{\sum_{G=1}^{4} \tilde{u}_G A_G \rho_G}{\sum_{G=1}^{4} A_G \rho_G}, \quad v = \frac{\sum_{G=1}^{4} \tilde{v}_G A_G \rho_G}{\sum_{G=1}^{4} A_G \rho_G}$$

where, A_G is the area in which the virtual grid covers each Eulerian grid, and $\tilde{u}_G$, $\tilde{v}_G$ and ρ_G are the Lagrangian velocities and densities of the corresponding grids. The coordinates $(\tilde{r}, \tilde{z})$ of transitional markers can be obtained as follows

$$\begin{bmatrix} \tilde{r} \\ \tilde{z} \end{bmatrix}^{n+1} = \begin{bmatrix} r \\ z \end{bmatrix}^{n} + \Delta t \begin{bmatrix} u \\ v \end{bmatrix}^{n}$$

Second, based on the order of markers at time t_n, transitional markers are connected, and the intersection points between the connecting line of two adjacent transitional markers and Eulerian grid line are sought to serve as markers at time t_{n+1}.

3.2 Numerical Simulation of Shaped Charge Jet

1) Numerical method

As for the simulation of shaped charge jet, governing equations of hydro-elastoplastic model consist of the mass conservation, the momentum conservation, the energy conservation, and the equation of state. These partial differential equations form a two-dimensional unsteady problem of isothermal inviscid compressible fluid without body force [Ma, Wang and Ning (2008); Wang, Huang and Ning (2009)]. The governing equations are discretized by an operator splitting technique [Benson (1995); Ma, Wang and Ning (2008)]. In the operator splitting method, the calculation involves two steps. The first step is a Lagrangian step in which the grid is allowed to distort with the material. In this step the changes in velocity and internal energy due to the pressure and deviatoric stress terms are calculated. In the second advection step, transport of mass, internal energy and momentum across grid boundaries is computed. This may be thought of as remapping the distorted mesh at the end of Lagrangian step back to the fixed Eulerian frame. Interface tracking algorithm is employed to track the material interface in the Eulerian step.

2) Numerical results of shaped charge jet formation

Liner cone angle, wall thickness and initiation mode have much effect on shaped charge jet, so the numerical simulation is performed to investigate the influences

of these factors on jet. The charge is B explosive and JWL equation of state is taken for the explosive and explosive products. The material of the liner is 45# steel and we can take Grüneison equation of state in the simulation. Because the whole model is featured axisymmetry, one-half model is established for obtaining the numerical solutions.

(1) Influence of liner cone angle on jet formation

Fig.9 illustrates shaped charge jet formation process for different liner conical angle. The tip velocity of jet for different liner cone angle is shown in Table 1. Table 2 lists comparison of numerical results and experiment ones for the tip velocity of the jet when liner cone angle is 60^o. It can be shown that the numerical results are in good agreement with the experimental data. It indicates that the numerical method proposed in this paper is efficient for the simulation of shaped charge jet.

Table 1: Numerical results of shaped charge jet for different liner cone angle

Jet parameter	Liner cone angle(^{o})				
	60	80	100	120	140
Tip velocity of jet(m/s)	5158.3	4326.6	3502.5	2828.9	2502.6

Table 2: Comparision between numerical result and experimental one for the tip velocity of jet

Parameter	Experimental result	Numerical result	Error
Tip velocity (m/s)	5275.2	5158.3	2.2%

It can be observed from the numerical results that when the conical angle of the liner increases, the tip velocity of jet decreases, the length of jet becomes shorter, and the diameter of jet becomes larger, which is consistent with the jet formation theory. This can be explained that the initial pressure on the surface of the liner is related to the included angle between the detonation wave front and the surface of liner. With the decrease the liner conical angle, the included angle will decrease, and the detonation load will increase, which leads to the increase of the collapse velocity of the liner element. Therefore, the shaped charge with smaller liner conical angle can form a jet with higher velocity.

(2) Influence of liner wall thickness on jet formation

Fig.10 illustrates shaped charge jet formation images under different liner wall thickness when liner cone angle is 120^o. Numerical results of jet parameters are shown in Table 3. It can be observed from the table and figures that when liner wall

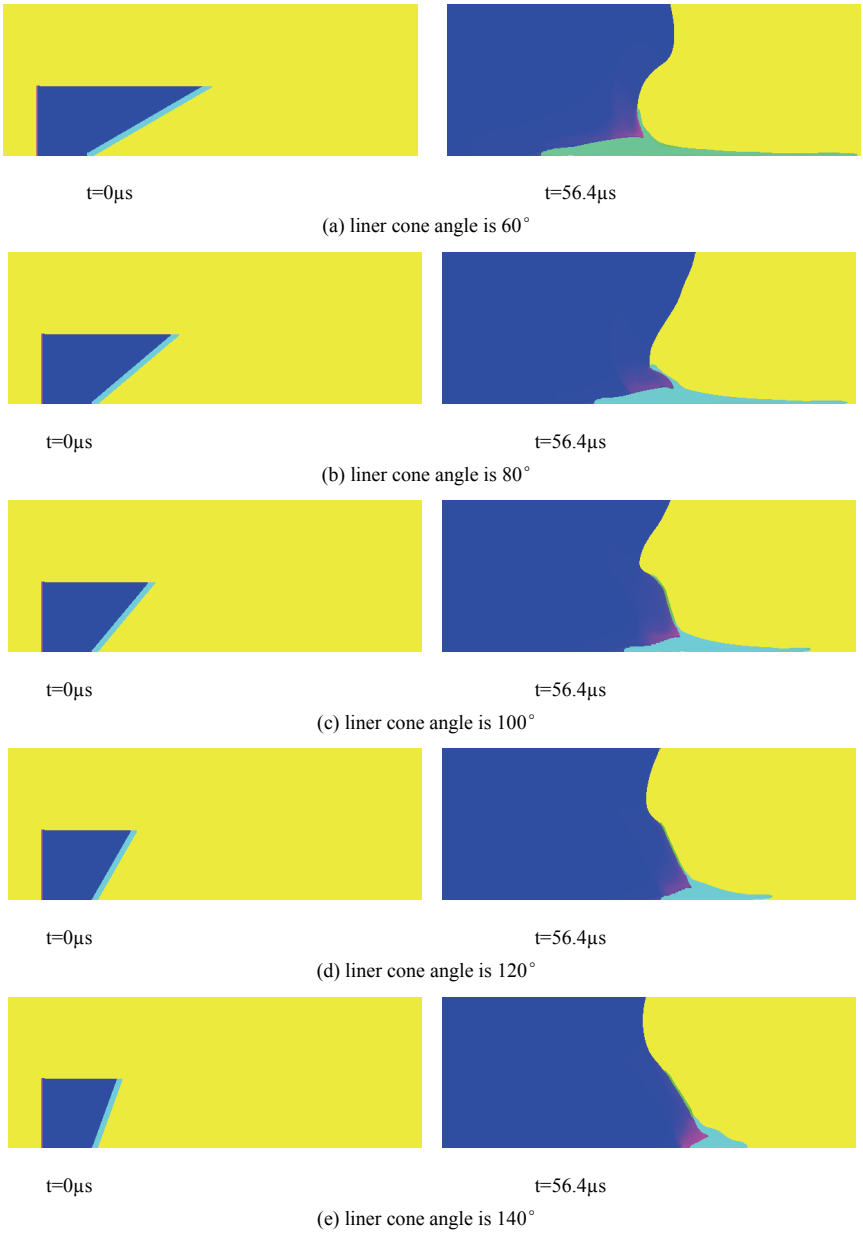

Figure 9: Shaped charge jet formation image for different liner conical angle

thickness increases, the tip velocity of jet decreases, the diameter of jet increases and the length of jet decreases. As a result of increased liner wall thickness, the liner mass increases. If the explosive mass will not change, the mass ratio of the explosive and liner drops. It is known from Gurney formulas that, the collapse velocity of liner element will decrease, and the tip velocity of the jet will drop accordingly.

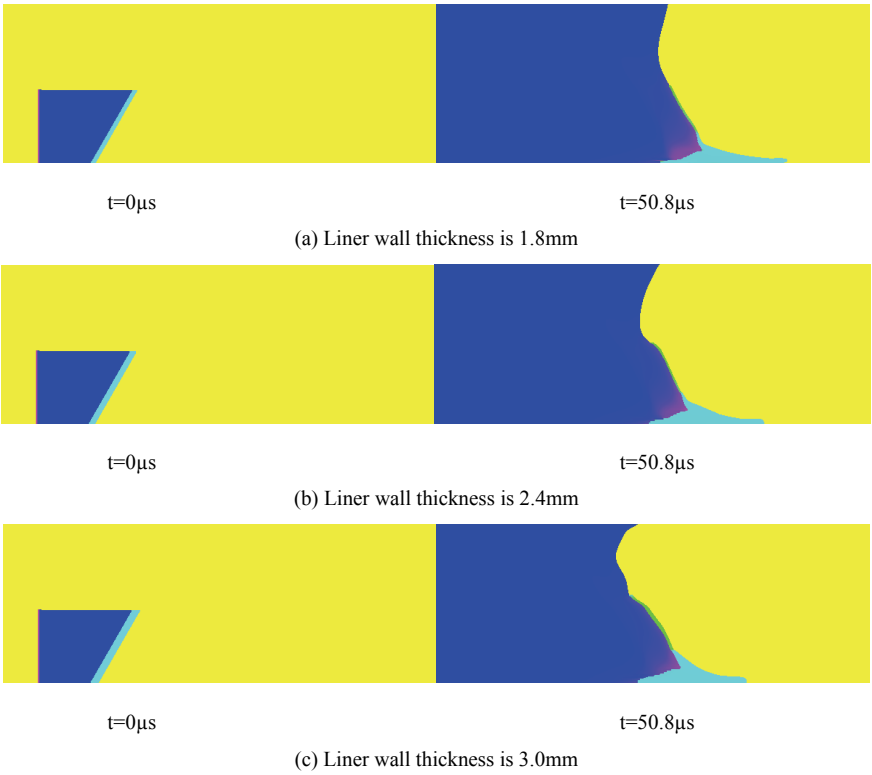

Figure 10: Shaped charge jet formation image for different liner wall thickness

(3) Influence of initiation mode on jet formation

Fig.11 illustrates shaped charge jet formation images under different initiation mode when liner cone angle is 120^o. Numerical results of jet parameters are demonstrated in Table 4. It can be observed from the table and figures that tip velocity for annular initiation is the highest, that for plane initiation comes second, and that for point initiation is the lowest. This is because the initial pressure imposed on the liner surface is considerably related to the included angle between the detonation

Table 3: Numerical results for different liner wall thickness

Jet parameters	Wall thickness of liner(mm)		
	1.8	2.4	3.0
Tip velocity of jet(m/s)	3183.5	2828.9	2665.4
Jet diameter(mm)	11.37	13.82	16.13
Jet length(mm)	69.6	62.8	59.2

wave front and liner generatrix. The Èýsmaller α angle, the larger the explosive load imposed on the liner element. Consequently, the collapse velocity of the liner element increases, which leads to an increase of the jet velocity. Fig.12 shows the included angles between liner generatrix and the detonation wave front for different initiation modes. $\alpha 1$, $\alpha 2$ and $\alpha 3$ are corresponding to annular initiation, plane initiation and point initiation, respectively. Clearly, $\alpha 1<\alpha 2<\alpha 3$, that is, the detonation load formed by annual initiation is the largest, its collapse velocity is the largest, and as a result the jet velocity is the largest. The axial-symmetric detonation waves which are produced by annual initiation collide at the charge axle and hence a high-pressure zone will be formed at the point of detonation wave collision. It will contribute to the increase of jet velocity as well.

Table 4: Numerical results of jet for different initiation mode

Jet parameters	Point Initiation	Plane initiation	Annular initiation
Tip velocity(m/s)	2466.7	2828.9	3053.0

4 Concluding remarks

1) The blockage ratio of obstacles exerts some influence on both flame velocity and pressure. Flame velocity rises as blockage ratio increases. When blockage ratio increases to a certain value, flame velocity begins to decline. Explosion overpressure increases with rising blockage ratio in an almost linear trend. Furthermore, the relationships of the propagation speed of the flame and explosion overpressure with blockage ratio are obtained by the regression analysis of the data .

2) Numerical simulation results indicate that, the spacing of obstacles has some influence on the explosion characteristics. If the spacing between obstacles is too close, after shock wave passes through two obstacles, the gas between the two obstacles is not yet combusted completely, which leads to inadequacy of the energy of shock wave. If the spacing is too large, the shock wave that is accelerated after passing through the first obstacle will be weakened due to dissipation before

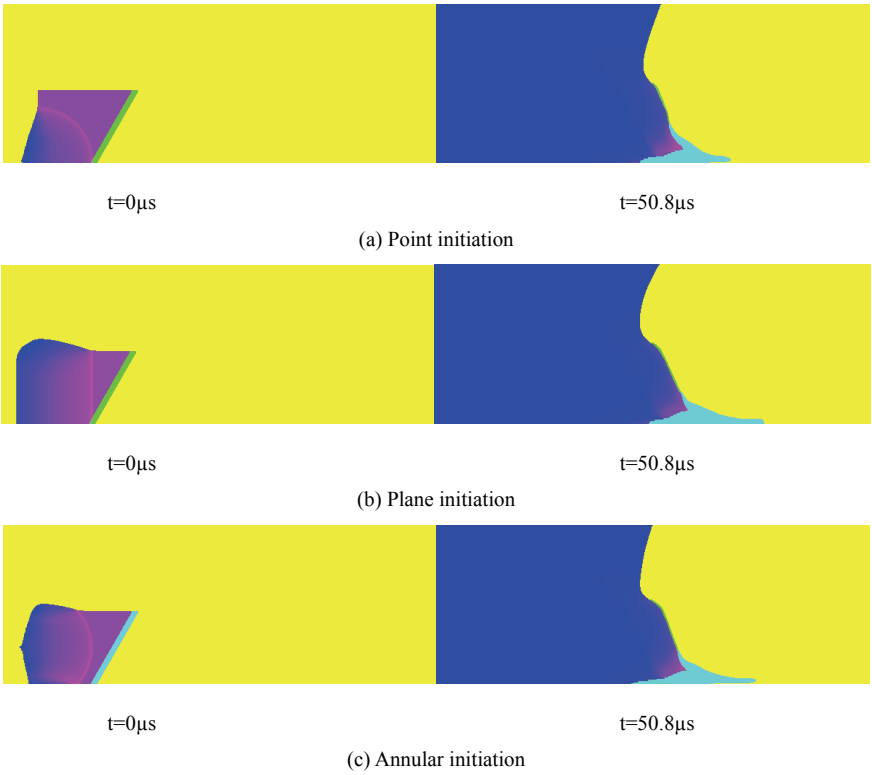

Figure 11: Shaped charge jet formation image for different initiation mode

it arrives to the next obstacle. The spacing which is close to the length of cellular structure of detonation wave λ is the most ideal distance for detonation wave propagation.

3) Based on the Steger-Warming vector flux splitting method, a splitting method is employed when the vector flux does not satisfy the homogeneity property for simulating detonation wave propagation for condensed explosives. The numerical results are in agreement with the physical image.

4) The multi-material Eulerian hydrocode that can effectively simulate shaped charge jet formation is developed. An interface treatment method is proposed for mixed cells, in which the interface for each material is traced by a series of straight-line segments connected head to tail and the end points of each straight-line segment are located on the grid lines. The numerical results indicate that the numerical method and hydrocode developed is feasible and efficient for the simulation of engineering

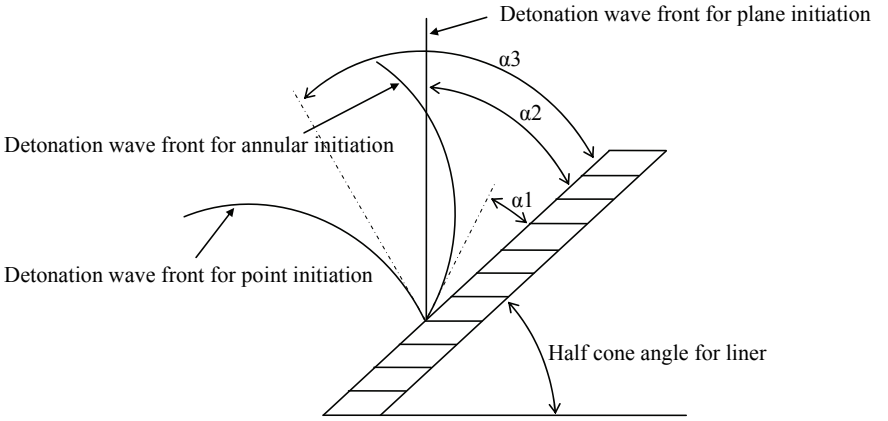

Figure 12: Scheme for included angle between detonation wave front and liner generatrix

problems.

Acknowledgement: This work is supported by Program for New Century Excellent Talents in University under grant number NCET-08-0043, National Nature Science Foundation of China under grant number 10972040 and the Foundation of State Key Laboratory of Explosion Science and Technology (Grant No. YBKT09-06).

References

Atluri, S.N., Shen, S.P. (2002): The meshless local Petrov-Galerkin (MLPG) method: A simple & less-costly alternative to the finite element and boundary element methods, *CMES: Computer Modeling in Engineering and Sciences*, vol. 3, No.1, pp. 11-51

Atluri, S. N.; Han, Z. D.; Rajendran, A. M. (2004): A New Implementation of the Meshless Finite Volume Method, Through theMLPG "Mixed" Approach, *CMES: Computer Modeling in Engineering & Sciences*, vol. 6, No.6, pp. 491-514.

Bardenhagen, S. G.; Kober, E. M. (2004): The generalized interpolation material point method, *CMES: Computer Modeling in Engineering & Sciences*, vol.5, No.6, pp. 477-495.

Benson, D.J. (1995): A multi-material Eulerian formulation for the efficient solution of impact and penetration problems, *Comput Mech*, Vol. 15, No. 6, pp.558–571.

Campbell, J.C.; Vignjevic, R.; Patel, M.; Milisavljevic, S. (2009): Simulation of Water Loading On Deformable Structures Using SPH, *CMES: Computer Modeling in Engineering & Sciences*, vol. 49, No.1, pp. 1-21.

Fedkiw, R.P.; Aslam, T.; Merriman, B.; Osher, S. (1999): A non-oscillatory Eulerian approach to interfaces in multimaterial flows (the ghost fluid method). *J Comput Physics*, Vol. 152, No. 2, pp. 457–492.

Fujiwara, T.; Taki, S. (1978): Numerical Analysis of Two-Dimensional Non-steady Detonations. *AIAA*. Vol. 16, No. 1, pp.73-77.

Gamezo, V. N.; Ogawa, T.; Elaine S. O. (2007): Numerical simulations of flame propagation and DDT in obstructed channels filled with hydrogen-air mixture. Proceedings of the Combustion Institute Vol. 31, No.2, pp. 2463-2471.

Gamezo, V. N.; Ogawa, T.; Elaine S. O. (2008): Flame acceleration and DDT in channels with obstacles: Effect of obstacle spacing. *Combust Flame*, Vol. 155, No. 1-2, pp. 302-315.

Han Z. D.; Rajendran, A. M; Atluri, S. N. (2005): Meshless Local Petrov-Galerkin (MLPG) Approaches for Solving Nonlinear Problems with Large Deformation and Rotation, *CMES: Computer Modeling in Engineering & Sciences*, vol. 10, No. 1, pp. 1-12.

Han, Z. D.; Liu, H. T.; Rajendran, A.M.; Atluri, S. N.(2006): The applications of meshless local Petrov-Galerkin (MLPG) approaches in high-speed impact, penetration and perforation problems. *CMES: Computer Modeling in Engineering & Sciences*, Vol. 14, No. 2, pp. 119-128.

Hirt, C. W.; Nichols, B. D. (1981): Volume of Fluid (VOF) Method for the Dynamics of Free Boundaries. *J Comput Physics*, Vol. 39, No.1, pp. 201-225.

Huang, P.; Zhang, X.; Ma, S.; Wang, H.K. (2008): Shared Memory OpenMP Parallelization of Explicit MPM and Its Application to Hypervelocity Impact, *CMES: Computer Modeling in Engineering & Sciences*, vol. 38, No.2, pp. 119-147.

Jiang, G. S.; Shu, C. W. (1996): Efficient implementation of weighted ENO schemes. *J Comput Physics*, Vol. 126, No.1, pp.202-228.

Kapila, A. K.; Schwendeman, D.W.; Bdzil, J. B.; Henshaw, W. D. (2007): A study of detonation diffraction in the ignition-and-growth model. *Combust Theor Model*, vol. 11, No. 5, pp. 781–822.

Lee, E.L.; Tarver, C.M.(1980): Phenomenological model of shock initiation in heterogeneous explosives. *Physics of Fluids*, Vol. 23, No.12, pp. 2362–2372.

Liu, T.G.; Khoo, B.C.; Yeo, K.S.(2003): Ghost fluid method for strong shock impacting on material interface. *J Comput Physics*, Vol. 190, No.2, pp. 651–681.

Ma, J.; Wang, B.; Lu, H.; Roy, S.; Hornung, R.; Wissink, A.; Komanduri, R. (2005): Multiscale Simulations Using Generalized Interpolation Material Point (GIMP) Method And SAMRAI Parallel Processing, *CMES: Computer Modeling in Engineering & Sciences*, vol. 8, No.2, pp. 135-152.

Ma, S.; Zhang, X.; Lian, Y. P.; Zhou, X. (2009): Simulation of high explosive explosion using adaptive material point method, *CMES: Computer Modeling in Engineering & Sciences*, vol.39, No.2, pp. 101-123.

Ma, T. B.; Wang C.; Ning J. G.(2008): Multi-material Eulerian Formulations and Hydrocode for the Simulation of Explosions. *CMES: Computer Modeling in Engineering & Sciences*, Vol. 33, No. 2, pp. 155-178.

Ning, J. G.; Wang, C.; Lu, J.(2006): Explosion characteristics of coal gas under various initial temperatures and pressures. *Shock Waves.* Vol. 15, No.6, pp. 461–472.

Osher, S.; Sethian J. A. (1998): Fronts propagating with curvature dependent speed: algorithms based in Hamilton–Jacobi formulations, *J Comput Physics*, Vol. 79, No.1, pp.12–49.

Rider, W. J.; Kothe D. B.(1998): Reconstructing Volume Tracking, *J Comput Physics*, Vol. 141, No.2, pp. 112-152.

Shen, L.M. (2009): A Rate-Dependent Damage/Decohesion Model for Simulating Glass Fragmentation under Impact using the Material Point Method, *CMES: Computer Modeling in Engineering & Sciences*, vol.49, No.1, pp. 23-45.

Shu, C. W. (2009): High Order Weighted Essentially Nonoscillatory Schemes for Convection Dominated Problems, *SIAM Rev*, Vol. 51, No.1, pp. 82-126

Stewart, D. S.; Yoo S.; Wescott B. L.(2007): High-order numerical simulation and modelling of the interaction of energetic and inert materials. *Combust Theor Model*, Vol. 11, No. 2, 305–332.

Steger, J. L.; Warming, R. F. (1981): Flux vector splitting of the inviscid gasdynamics equations with application to finite-difference methods. *J Comput Physics*, Vol.40, No.2, pp.263-293.

Sun, J. S; Zhu J. S.(1995): Theoretical Explosion Physics, Defense Industry Press, Beijing

Tran, B.; Udaykumar, H. S. (2004): A particle-level set-based sharp interface cartesian grid method for impact, penetration, and void collapse. *J Comput Physics*, Vol.193, No.2, pp.469-510

Vaagsaether, K.; Knudsen, V.; Bjerketvedt D. (2007): Simulation of flame ac-

celeration and DDT in H_2-air mixture with a flux limiter centered method. *Int J Hydrogen Energ*, Vol.32, No.13, pp.2186 – 2191.

Wang, C.; Huang, F. L.; Ning J. G.(2009): Jet Formation and Penetration Mechanism of W Typed Shaped Charge. *Acta Mech Sinica*, Vol. 25, No.1, pp.107-120

Wang, J. T.; Liu, K. X.; Zhang, D. L.(2009): An improved CE/SE scheme for multi-material elastic–plastic flows and its applications. *Computers & Fluids.* Vol.38, No.3, pp.544-551

Wen, W. Z. (1998): Marker on Cell Line (MOCL) and It's Application in Numerical Simulations. Doctoral thesis, Beijing Institute of Technology.

Xu, S. J.; Aslam, T.; Stewart, D. S.(1997): High resolution numerical simulation of ideal and non-ideal compressible reacting flows with embedded internal boundaries. *Combust Theor Model*, Vol.1, No.1, pp. 113–142.

Stewart, D. S.; Yoo, S.; Wescott, B. L. (2007): High-order numerical simulation and modelling of the interaction of energetic and inert materials. *Combust Theor Model*, Vol.11, No.2, pp.305–332.

Youngs, D. L. (1982): Time-DependentMulti-Material Flow with Large Fluid Distortion. In: Morton, K. W. and Baines, M. J. (ed) *Numerical Methods for Fluid Dynamics*, Academic Press, New York, pp. 273-285.